JOURNAL OF GEOPHYSICAL RESEARCH, VOL. 114, D08303, doi:10.1029/2008JD010621, 2009

Transport pathways of carbon monoxide in the Asian summer monsoon diagnosed from Model of Ozone and Related Tracers (MOZART)

Mijeong Park,[1] William J. Randel,[1] Louisa K. Emmons,[1] and Nathaniel J. Livesey[2]

Received 17 June 2008; revised 13 January 2009; accepted 16 February 2009; published 22 April 2009.

[1] Satellite observations of tropospheric chemical constituents (such as carbon monoxide, CO) reveal a persistent maximum in the upper troposphere–lower stratosphere (UTLS) associated with the Asian summer monsoon anticyclone. Diagnostic studies suggest that the strong anticyclonic circulation acts to confine air masses, but the sources of pollution and transport pathways to altitudes near the tropopause are the subject of debate. Here we use the Model for Ozone and Related Tracers 4 (MOZART-4) global chemistry transport model, driven by analyzed meteorological fields, to study the source and transport of CO in the Asian monsoon circulation. A MOZART-4 simulation for one summer is performed, and results are compared with satellite observations of CO from the Aura Microwave Limb Sounder and the Atmospheric Chemistry Experiment Fourier Transform Spectrometer. Overall, good agreement is found between the modeled and observed CO in the UTLS, promoting confidence in the model simulation. The model results are then analyzed to understand the sources and transport pathways of CO in the Asian monsoon region, and within the anticyclone in particular. The results show that CO is transported upward by monsoon deep convection, with the main surface sources from India and Southeast Asia. The uppermost altitude of the convective transport is ~12 km, near the level of main deep convective outflow, and much of the CO is then advected in the upper troposphere northeastward across the Pacific Ocean and southwestward with the cross-equatorial Hadley flow. However, some of the CO is also advected vertically to altitudes near the tropopause (~16 km) by the large-scale upward circulation on the eastern side of the anticyclone, and this air then becomes trapped within the anticyclone (to the west of the convection, extending to the Middle East). Within the anticyclone, the modeled CO shows a relative maximum near 15 km, in good agreement with observations.

Citation: Park, M., W. J. Randel, L. K. Emmons, and N. J. Livesey (2009), Transport pathways of carbon monoxide in the Asian summer monsoon diagnosed from Model of Ozone and Related Tracers (MOZART), *J. Geophys. Res.*, *114*, D08303, doi:10.1029/2008JD010621.

1. Introduction

[2] Carbon monoxide (CO) is a principal pollutant in the troposphere, which plays an important role in the chemistry of the atmosphere and has an indirect radiative effect through its influence on ozone [*Marenco et al.*, 1994; *Novelli et al.*, 1998]. The main sources of CO are both natural and anthropogenic, including combustion processes near the surface (transport, power plants, domestic heating and biomass burning) and oxidation of methane and other nonmethane hydrocarbons. Overall, approximately half of the tropospheric burden of CO comes from photochemical production, and half from direct surface emissions [*Horowitz et al.*, 2003; *Duncan et al.*, 2007]. The main sink of CO is oxidation by the hydroxyl radical (OH) [*Logan et al.*, 1981]. Free troposphere concentrations of CO range from 50 parts per billion per volume (ppbv) in unpolluted areas to over 700 ppbv near emission sources [*Clerbaux et al.*, 2007].

[3] Because CO has a photochemical lifetime in the range of 2–3 months [*Xiao et al.*, 2007], it is useful as a tracer of transport in the troposphere and lower stratosphere [e.g., *Bowman*, 2006]. In situ observations of CO based on various measurement techniques are used to monitor long-term changes in the troposphere [*Novelli et al.*, 2003; *Nedelec et al.*, 2005; *Velazco et al.*, 2007]. Space-borne measurements of CO are especially useful in studying transport processes and convective influences on a global scale [*Connors et al.*, 1999; *Edwards et al.*, 2003, 2006]. Recent measurements of upper tropospheric CO from the Aura Microwave Limb Sounder (MLS) show evidence of long-range transport of CO from Asia [*Jiang et al.*, 2007].

[1] Atmospheric Chemistry Division, National Center for Atmospheric Research, Boulder, Colorado, USA.
[2] Jet Propulsion Laboratory, California Institute of Technology, Pasadena, California, USA.

0148-0227/09/2008JD010621$09.00

[4] The Asian monsoon anticyclone is the dominant circulation feature in the upper troposphere and lower stratosphere (UTLS) during Northern Hemisphere (NH) summer [*Hoskins and Rodwell*, 1995; *Highwood and Hoskins*, 1998]. Satellite observations show persistent high levels of tropospheric pollutants (such as CO and hydrogen cyanide, HCN) inside the anticyclone [*Li et al.*, 2005; *Park et al.*, 2007, 2008]. This enhancement is probably due to upward transport of pollutants in deep convection associated with the monsoon circulation, and confinement within the strong, closed circulation of the anticyclone [*Li et al.*, 2005; *Randel and Park*, 2006]. However, there have been different perspectives on how air parcels with sources in the lower troposphere reach the tropopause (which is near 16 km). This is due to the fact that the main level of deep convective outflow in the tropics is typically near 12 km [*Folkins et al.*, 2000], and the main route taken from this lower level to the tropopause is unclear. Overshooting convection is one mechanism to transport constituents up to the tropopause in the monsoon anticyclone [*Dessler and Sherwood*, 2004]. However, the frequency of overshooting convection that reaches the tropopause appears to be very low [*Gettelman et al.*, 2002; *Liu and Zipser*, 2005], and to date there is no direct way to quantify the effect of overshooting deep convection on transport in this region. Also, the persistent deep convection in the Asian monsoon is located over Southeast Asia, which is far from the center of the anticyclone where tracers show extreme values [*Park et al.*, 2007]. *Park et al.* [2007] have suggested that slow upward vertical motion is part of the balanced dynamical structure of the anticyclone in the upper troposphere, which could contribute to upward constituent transport above the level of maximum convective outflow. In a similar argument, *Folkins et al.* [2008] suggest a component of large-scale dynamical divergence that peaks above the level of deep convective outflow ($\sim$15 km) in the tropical Western Pacific.

[5] The focus of this study is to simulate and understand the transport of air parcels from the polluted surface up to the tropopause over the Asian monsoon anticyclone. We use a state-of-the-art global chemistry transport model (MOZART, version 4) to simulate CO during a particular NH summer (year 2005), based on assimilated meteorological fields and surface emission sources of CO. The model simulations are compared with satellite observations of CO obtained from the Aura MLS and the Atmospheric Chemistry Experiment Fourier Transform Spectrometer (ACE-FTS) in terms of spatial and temporal characteristics in the UTLS region. We then examine the detailed transport and chemistry of CO from the model simulation, in order to quantify the importance of regional CO sources over India and Southeast Asia, and also to understand the mechanisms for transport to the UTLS region.

2. Model and Data Description

2.1. Model Description

[6] The Model for Ozone and Related chemical Tracers (MOZART) is a global chemistry transport model developed at the National Center for Atmospheric Research, the NOAA Geophysical Fluid Dynamics Laboratory and the Max Planck Institute for Meteorology. MOZART-4 includes comprehensive tropospheric chemistry, simulating 97 chemical species and bulk aerosols (L. K. Emmons et al., Impact of Mexico City emissions on regional air quality from MOZART-4 simulations, manuscript in preparation, 2009, available at http://gctm.acd.ucar.edu/).

[7] For the simulation in this study, the model is driven by meteorological fields from the National Centers for Environmental Prediction/Global Forecast System (NCEP/GFS) for the time period June–September 2005. The horizontal resolution is 2.8° latitude by 2.8° longitude and the vertical grid has 42 sigma levels extending from the surface up to about 2 hPa. For levels above the tropopause, which is determined from the temperature profiles in the model, the CO tendency equation includes a relaxation to a stratospheric zonal average climatology. The climatology is derived from a stratospheric version of MOZART (MOZART-3) [see *Kinnison et al.*, 2007] and applied to the model with a 10-day relaxation time scale; this stratospheric forcing has almost no effect on the near-tropopause results shown here, as confirmed in a simulation where this relaxation was omitted. Outputs from the model runs are archived as daily averages, including all of the individual terms in the continuity equation for CO (as described in detail below).

[8] We also include analyses of MOZART-4 simulations where the total (natural and anthropogenic) sources of CO are tagged according to the surface emission regions. CO emissions included in this study are based on the Precursors of Ozone and their Effects in the Troposphere (POET) inventory for 2000 (C. Granier et al., POET, a database of surface emissions of ozone precursors, 2005, available at http://www.aero.jussieu.fr/projet/ACCENT/POET.php). The anthropogenic emissions, i.e., emissions from fossil fuel combustion (cars, power plants, etc.), biofuel combustion (domestic heating and cooking), over Asia have been updated with the inventory developed by D. Streets (Argonne National Laboratory) for the NASA/INTEX-B experiment http://www.cgrer.uiowa.edu/EMISSION_DATA_new/index_16.html). The biomass burning emissions (specific for the year of the simulation) are from the Global Fire Emissions Database (GFED-2) [*van der Werf et al.*, 2006]. The natural sources of CO from ocean and soil are much less than the other sources.

[9] For comparisons with the MLS satellite observations, the MOZART-4 simulated CO mixing ratio is interpolated to the MLS pressure levels. We have also made comparisons using the model output weighted with the approximate vertical weighting of the MLS instrument, and the results are very similar to the pressure level comparisons shown here. The ACE-FTS data is compared at the approximate altitude levels close to the MLS pressure levels in the tropics.

2.2. Satellite Data

[10] The Aura MLS [*Waters et al.*, 2006] is one of four instruments onboard NASA's Aura spacecraft, which was launched on 15 July 2004 [*Schoeberl et al.*, 2006]. MLS observes thermal microwave limb emission from broad spectral bands from 118 GHz to 2.5 THz using limb viewing geometry. It has a near-polar orbit and provides daily global coverage with $\sim$14 orbits per day. The standard product for CO is taken from the 240 GHz retrieval and is

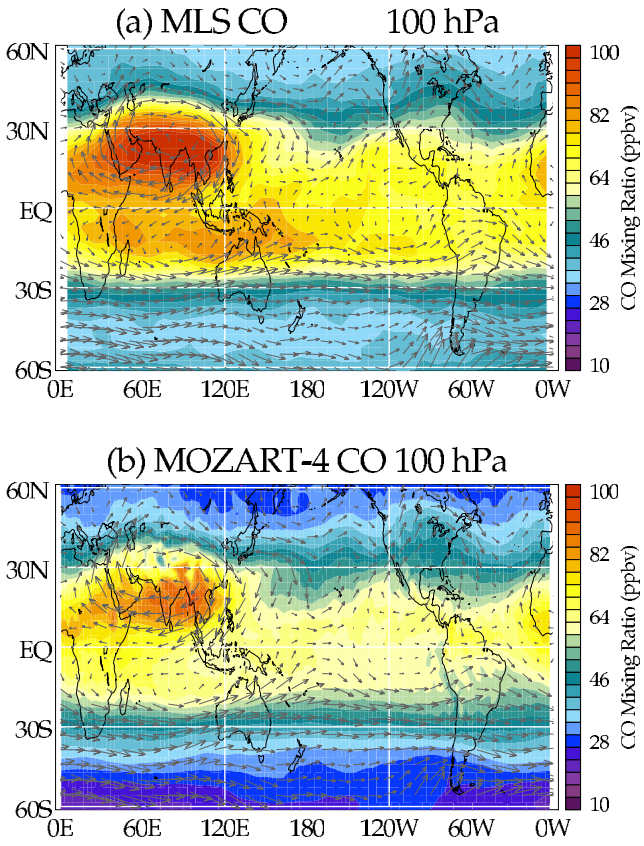

Figure 1. Horizontal structure of carbon monoxide (CO) for (a) MLS and (b) MOZART-4 at 100 hPa in June 2005. Horizontal wind vectors from the National Centers for Environmental Prediction/National Center for Atmospheric Research (NCEP/NCAR) reanalysis and the National Centers for Environmental Prediction/Global Forecast System (NCEP/GFS) analysis are overlaid, respectively.

reported on a fixed vertical pressure having 6 levels per decade ($10^{-n/6}$ hPa) starting at 1000 hPa.

[11] The CO observations used here are based on MLS retrieval version 2.2 (v2.2), covering the period June–September 2005. The vertical resolution for CO is ~4.5 km in the UTLS region, and we focus here on results for pressure levels 100 hPa and 215 hPa. The root mean square average of the estimated precision for CO is 15–40 ppbv in the UTLS region [*Livesey et al.*, 2007] (available at http://mls.jpl.nasa.gov). Comparisons with other data sets suggest that the v2.2 MLS CO data has relatively small mean bias at 100 hPa (±20 ppbv, with a scatter of ~±10 ppbv), but has a substantial high bias at 215 hPa (by possibly a factor of two) [see *Livesey et al.*, 2008]. On account of this bias, we include an explicit factor of two for the 215 hPa MLS data comparisons shown below (as noted in the figure captions). We construct a gridded data set from the MLS observations on 5° latitude by 10° longitude grids by averaging available profiles inside each bin every 2 days. For more details of the MLS CO data used in this study, see *Park et al.* [2007].

[12] We also use CO satellite observations obtained from the ACE-FTS instrument for the period from June to August 2004–2006. ACE-FTS measures solar absorption spectra from 750 to 4400 cm^{-1} using solar occultation technique [*Bernath et al.*, 2005]. The vertical field of view of the instrument is 3 km, with somewhat higher resolution in the UTLS (~2–3 km) afforded by oversampling; the vertical spacing of the retrieval grid is 1 km. We use CO from ACE-FTS version 2.2, with an estimated uncertainty of 2–6% in the UTLS region [*Clerbaux et al.*, 2007]. The ACE satellite primarily provides measurements over high latitudes, with relatively infrequent sampling over the Asian monsoon region. However, there are enough observations over this region during the years 2004–2006 to build up a statistical picture of CO (and other tropospheric constituents) in the UTLS during summer [*Park et al.*, 2008], and we use these results for additional, independent comparisons to the MOZART-4 simulation.

3. Comparison of MOZART Simulations With Satellite Measurements

[13] Monthly mean CO mixing ratios from the MOZART simulation at 100 hPa are compared to the MLS CO measurements in Figure 1 for June 2005, and similar comparisons are shown for the 215 hPa level in Figure 2. The horizontal wind vectors for the corresponding pressure levels plotted on the MLS and MOZART maps are from the National Center for Environmental Prediction/National Center for Atmospheric Research (NCEP/NCAR) reanalysis [*Kistler et al.*, 2001] and NCEP/GFS analysis, respectively. Note that the MOZART and MLS color scales are identical

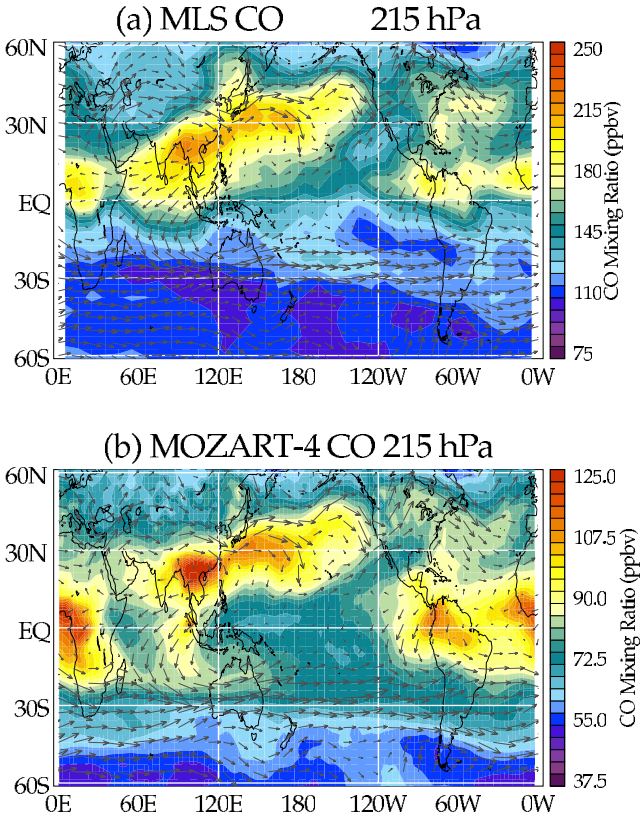

Figure 2. Same as Figure 1, but for 215 hPa. Note that the color scale for the Aura Microwave Limb Sounder (MLS) data is twice that for the model, to account for the approximate factor of 2 high bias in the MLS data at 215 hPa.

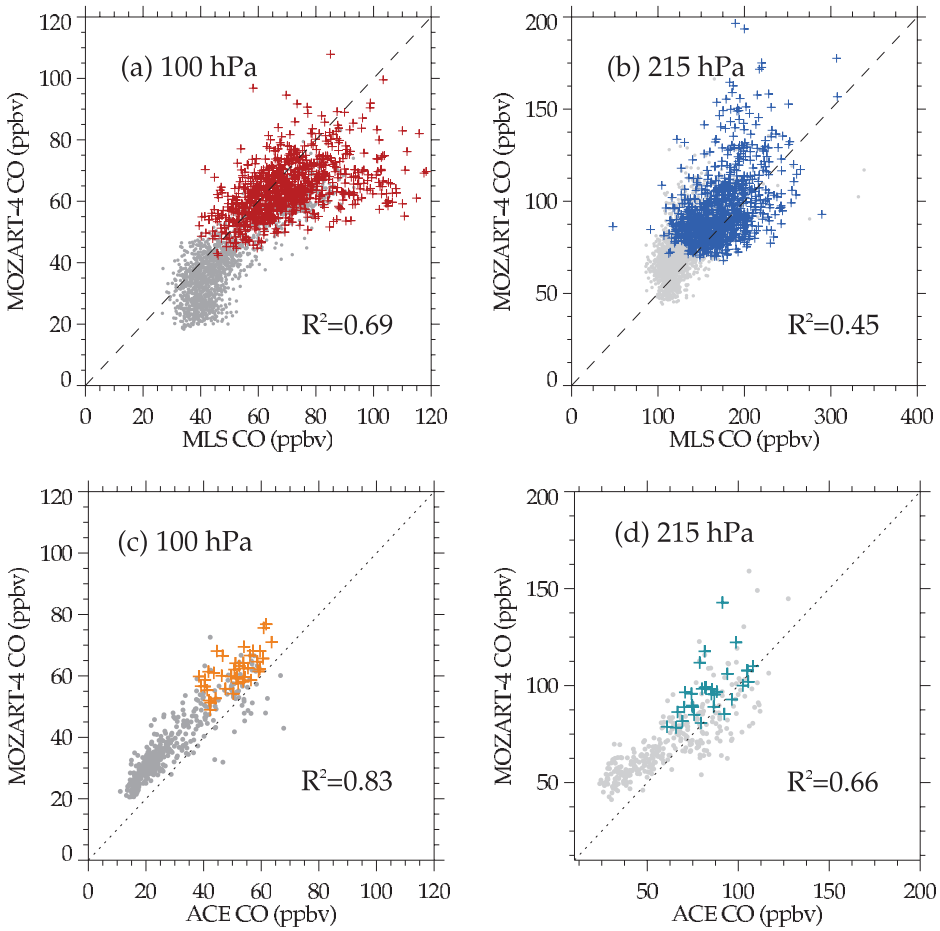

Figure 3. (top) Scatterplots of MLS versus MOZART-4 CO subsampled on 40° × 20° (longitude × latitude) grids between 60°S and 60°N from June to August 2005: (a) 100 hPa and (b) 215 hPa. Note that the scale for MLS data at 215 hPa is doubled compared to the MOZART results, to account for the approximate factor of 2 high bias in the MLS data at this level. (bottom) Scatterplots of the Atmospheric Chemistry Experiment Fourier Transform Spectrometer (ACE-FTS) versus MOZART-4 CO sampled at the ACE observation locations for the same period: (c) 100 hPa and (d) 215 hPa. Colored symbols represent measurements between 0° and 30°N latitude and over all longitudes.

for the 100 hPa level (Figure 1), but differ by a factor of two for the 215 hPa level (Figure 2), to account for the approximate factor of two high bias in the MLS retrieval at this level. MLS shows a broad maximum in CO over the Asian monsoon anticyclone at 100 hPa (Figure 1a), and the MOZART results (Figure 1b) show an overall agreement of this maximum (with a slightly reduced magnitude within the anticyclone and in the tropics). At 215 hPa (Figure 2a) the spatial structure of MLS CO is somewhat different than 100 hPa, with areas of enhanced CO corresponding to regions of persistent deep tropical convection (primarily over the Asian monsoon region, and also over South America and Africa). There is an extension of the Asian maximum over the North Pacific Ocean, which results from long-range transport of pollution lofted in deep convection [*Jiang et al.*, 2007], and there is also evidence of transport southward from the convective region in the cross-equatorial Hadley circulation. Similar overall structure at 215 hPa is observed in the MOZART-4 simulation (Figure 2b), although the large-scale latitudinal gradient across the Southern Hemisphere (SH) westerlies is weaker than observed. Overall, the comparisons in Figures 1–2 suggest that MOZART-4 provides a qualitatively reasonable simulation of the global distribution of CO during NH summer (June–August 2005) in the UTLS region.

[14] Figure 3 shows scatterplots of CO from MOZART-4 versus MLS and ACE-FTS at 100 and 215 hPa, respectively, derived from colocated samples during June–August 2005. The MLS data are sampled at every fourth grid point (to limit the number of samples to ~2,500), while all 420 of the ACE-FTS observations for this period are included. To highlight the monsoon regions, we show measurements between 0° and 30°N as colored symbols, and the rest of the points between 60°S and 60°N are shown as gray dots. Overall there is strong correlation between MOZART-4 and ACE-FTS CO at both pressure levels, with the suggestion of a small high bias in MOZART. The MOZART-MLS correlations show reasonable agreement at 100 hPa, although the MLS data are systematically higher than the simulation for the highest values. Taking into consideration the factor of two bias of the MLS data, there is overall agreement

between MLS and MOZART-4 CO at 215 hPa (Figure 3b), although the correlation is lower.

[15] Figure 4 shows further quantitative comparisons of the MOZART-4 simulations of CO with both MLS and ACE-FTS data, using probability density functions (PDFs) of all data over the NH subtropics (0°–30°N) at 100 and 215 hPa, respectively. The MLS and MOZART-4 results are for June–August 2005 and all the ACE-FTS measurements are included for June–August 2004–2006 to increase the number of available data. The three PDFs at 100 hPa (Figure 4a) show somewhat different peak values, with MLS data approximately 20 ppbv higher than ACE-FTS, and the MOZART-4 simulation in between. *Livesey et al.* [2008] suggest that MLS CO has higher uncertainties at 100 hPa, and efforts are being made to improve this in future versions of the data. Overall, very good agreement is found for comparisons at 215 hPa (Figure 4b), if the factor of two bias of the MLS retrievals is taken into account.

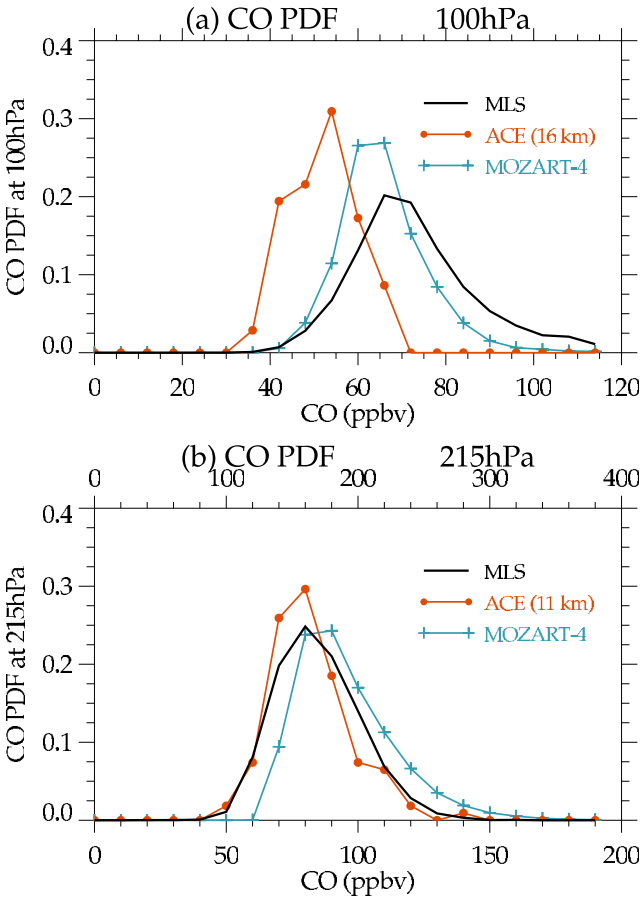

Figure 4. (a) Probability density functions (PDFs) of MOZART-4 CO (plusses) and MLS CO (solid line) at 100 hPa from June to August 2005 and ACE-FTS CO (solid circles) at 16 km in from June to August 2004–2006. (b) Same as Figure 4a, but for MOZART-4 and MLS CO at 215 hPa and ACE-FTS CO at 11 km. Measurements between 0° and 30°N latitudes are only counted. In Figure 4b, note that the MLS scale (top) is doubled compared to the ACE-FTS and MOZART scales, to account for a high bias in the MLS data.

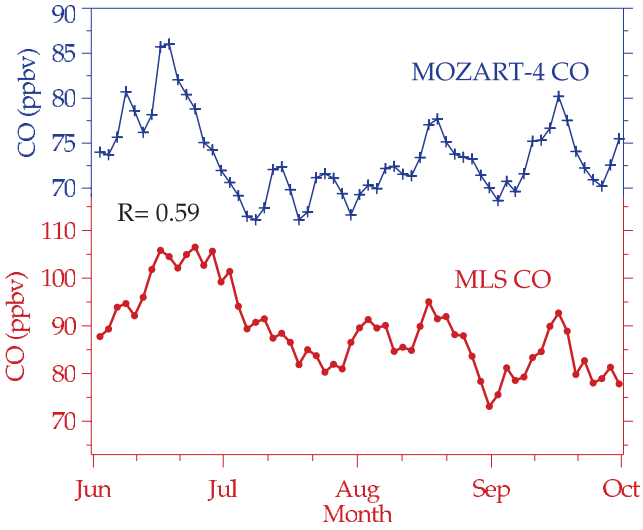

Figure 5. Time series of (top) MOZART-4 CO (ppbv) and (bottom) MLS CO (ppbv) at 100 hPa averaged in 20°–100°E/10°–30°N from June to September 2005.

[16] The synoptic variability of the MLS CO inside the Asian monsoon anticyclone is highly correlated to deep convection over Southeast Asia [*Park et al.*, 2007, Figure 8]. The boundary of the Asian monsoon anticyclone can be defined either dynamically [*Randel and Park*, 2006] or chemically [*Park et al.*, 2008]. Figure 5 shows time series of the MOZART-4 CO averaged over the region 20°–100°E longitudes and 10°–30°N latitudes, showing high correlation with the MLS CO time series in the same area. The separate episodes of enhanced CO seen in Figure 5 are linked to periods of enhanced convection, as shown in the work of *Park et al.* [2007].

[17] Figure 6 shows a comparison of the 100 hPa CO fields from MLS and MOZART-4 for one particular day (14 June, selected based on the CO maximum observed in Figure 5), and this also shows overall agreement (with slightly lower values in the maximum over the monsoon anticyclone and in the SH for the MOZART-4). Overall, the synoptic variability of the MOZART-4 CO shows reasonable agreement with the MLS CO observations, and in particular the strong convective events in June, August and September are reproduced in the model.

4. Transport Diagnostics

[18] The comparisons in Section 3 demonstrate that MOZART-4 provides a reasonable simulation of CO (both mean and variability) in the UTLS during NH summer, and here we focus on using the model results to understand the details of CO transport in the Asian monsoon region. As shown in Figure 1, the CO maximum at 100 hPa covers a wide region of Southeast Asia and the Middle East where the monsoon anticyclonic circulation is strong. On the other hand, at 215 hPa (Figure 2) the CO maximum is located over India and Southeast Asia, nearly overlying the region of maximum deep convection. The west side of the CO maximum at 100 hPa, as a result, is located far west of the maximum at 215 hPa (and convection). The characteristic difference in the east and the west sides of the anticyclone is highlighted in the vertical cross-sections of CO at longi-

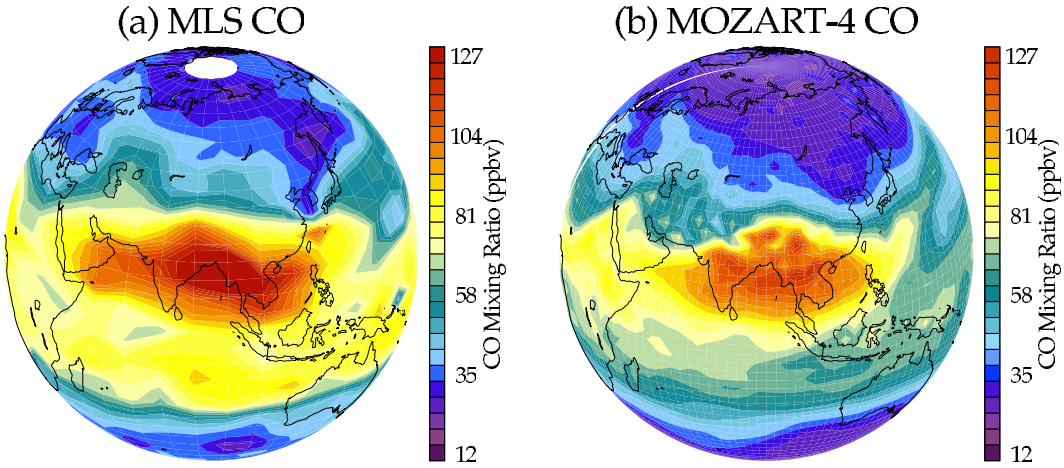

Figure 6. Synoptic map of CO at 100 hPa for (a) MLS and (b) MOZART-4 for 14 June 2005.

tudes of the western (67.5°E) and eastern side (112.5°E) of the anticyclone, as shown in Figure 7. On the eastern side (Figure 7b) there is a plume of high CO from the surface up to the tropopause near 30°N, with over 100 ppbv of CO found near 15 km between 10° and 30°N. In contrast, the western side (Figure 7a) exhibits an isolated maximum between ~12 to 16 km over low latitudes (0°–30°N). This structure results from the horizontal transport of CO in the uppermost troposphere to the west within the monsoon anticyclone circulation due to strong easterly jets [*Lelieveld et al.*, 2002]. This isolated maximum in the upper troposphere (Figure 7a) is similar to the vertical structure observed in CO and other tropospheric tracers inside the anticyclone from ACE-FTS data, which shows a maximum enhancement near the tropopause [*Park et al.*, 2008]. To better illustrate this behavior of CO, we show the average profiles of ACE-FTS and MOZART-4 CO in Figure 8, separated for locations inside and outside of the anticyclone, following the analysis of *Park et al.* [2008]. Overall there is reasonable agreement in the observed and modeled CO vertical profiles, and the profiles inside of the anticyclone show a distinctive vertical structure with a relative maximum near 15 km for both the model and observations.

[19] This characteristic behavior of CO over the monsoon anticyclone prompts several questions regarding vertical transport and the origin of CO in the upper troposphere. Specifically, (1) What regions of CO surface emissions contribute to the CO maximum inside the anticyclone at 100 hPa? (2) What are the mechanisms responsible for transport of CO to 100 hPa over the monsoon region in the model? (3) What is the relative importance of convection versus other transport processes, and how does this depend on location?

4.1. Origin of CO in the Upper Troposphere

[20] We address the first question by isolating the transport of specific surface sources of CO in MOZART-4 (so-called tagged sources). A map of the CO surface emissions used in the model for June 2005 (both natural and anthropogenic) is shown in Figure 9. The strongest CO surface

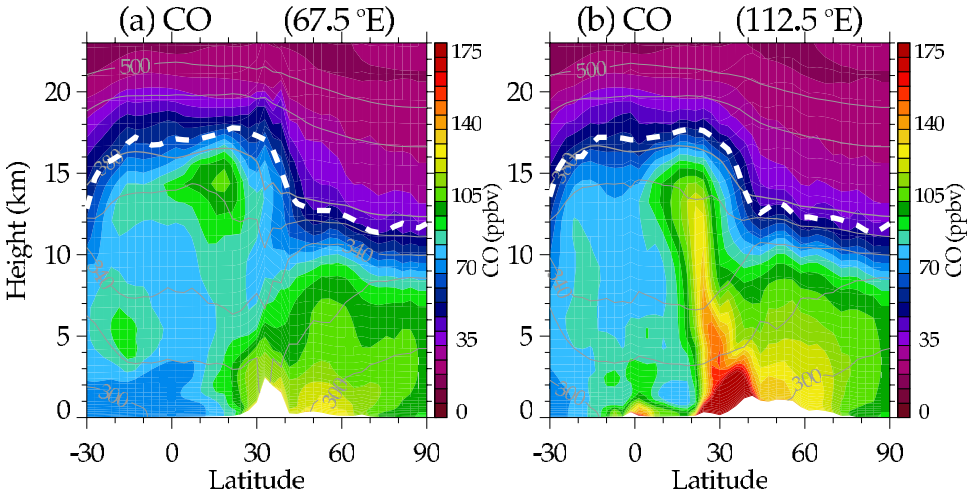

Figure 7. Latitude-altitude cross-sections of monthly mean MOZART-4 CO at the (a) western (67.5°E) and (b) eastern (112.5°E) sides of the monsoon maximum in June 2005. Thermal tropopause derived from the model temperature profile is denoted as thick dashed lines. Thin solid lines are isentropes (320, 340, 360, 380, 450, and 500 K).

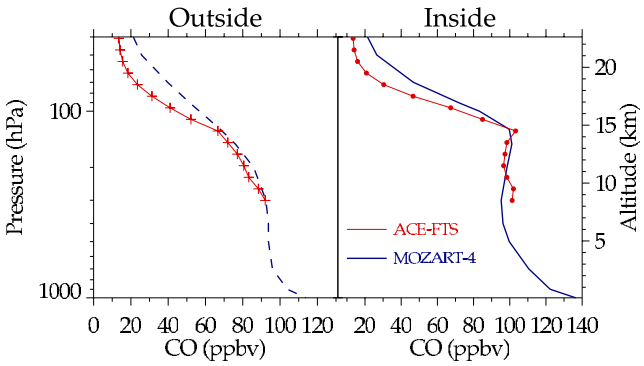

Figure 8. Average vertical profiles of MOZART-4 CO (June 2005) and ACE-FTS CO (June–August 2004–2006) (left) outside (dashed and plusses) and (right) inside (solid and circles) of the anticyclone, respectively.

emissions are found over East China (100°–120°E and 20°–40°N). CO emissions are relatively high over India and Southeast Asia, while there are low emissions west of India (70°E longitude) and over the Tibetan Plateau. The CO surface emissions over Asia used in this simulation vary little in time from June to September 2005 (figures not shown).

[21] The MOZART-4 simulation is performed with CO being tagged in three separate source regions: East China (region A, 100°–120°E/20°–40°N), India and Southeast Asia (region B, 60°–100°E/10°–30°N), and over the Tibetan Plateau (region C, 70°–100°E/30°–40°N) (see Figure 9). The Tibetan Plateau is added in the simulation because of its unique thermodynamic conditions and possible source of convection as discussed by *Fu et al.* [2006]. The distributions of CO at 100 hPa resulting from the tagged model run are shown in Figures 10a–10c. Most of the CO within and near the Asian monsoon anticyclone comes from India and

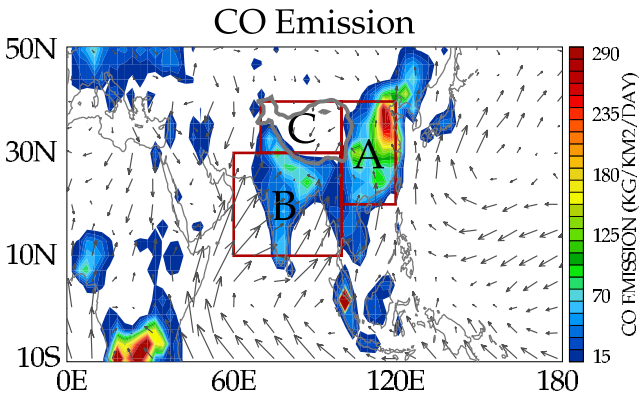

Figure 9. CO surface emissions (kg/km^2/d) included in the MOZART-4 simulation (color) and horizontal wind vectors at 1000 hPa from the NCEP/NCAR reanalysis in June 2005. Three geographical regions defined in the CO tagged run (A, East China, 100°–120°E/20°–40°N; B, India and Southeast Asia, 60°–100°E/10°–30°N; C, Tibetan Plateau, 70°–100°E/30°–40°N) are marked as red rectangles.

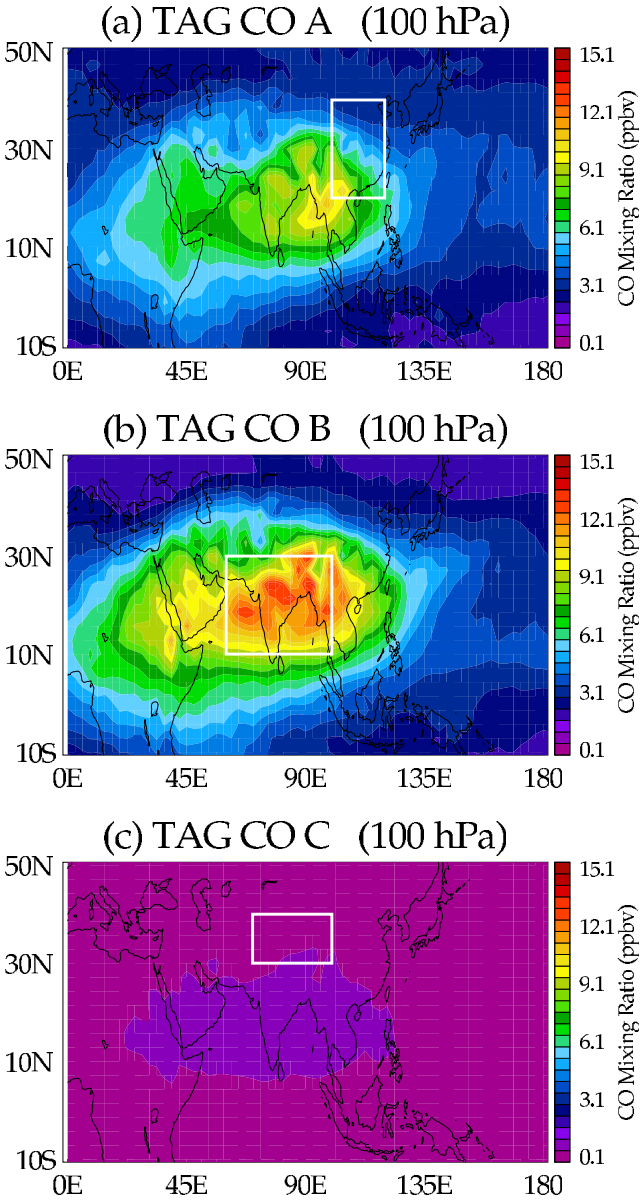

Figure 10. Horizontal structures of the MOZART-4 CO at 100 hPa as results of the CO tagged run: (a) East China, (b) India and Southeast Asia, and (c) Tibetan Plateau.

Southeast Asia (Region B, Figure 10b), whose maximum contribution accounts for over 60% of the total tagged CO at this altitude. There is also some smaller contribution from region A (Figure 10a), but insignificant addition from the Tibetan Plateau region (Figure 10c). The contribution from the rest of the globe is insignificant compared to the contribution from the regions A and B. Note that, on a global basis, CO originating from surface emissions constitutes about 50% of the CO concentration at 100 hPa, with the remainder resulting from chemical production in the troposphere.

4.2. Budget Analysis

[22] The mechanisms responsible for CO transport in the model can be studied by analyzing CO budgets in the

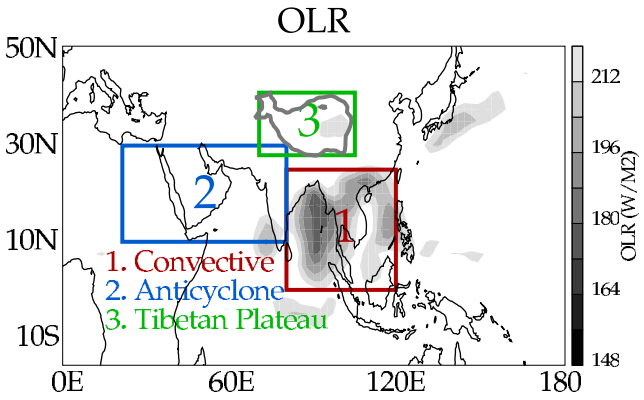

Figure 11. Geographical location of deep convection (OLR $\leq$ 212 W/m^2) and three regions defined in the budget analysis, i.e., region 1 (convective region, 80°–120°E/0°–25°N), region 2 (anticyclone region, 20°–80°E/10°–30°N), and region 3 (Tibetan Plateau, 70°–105°E/28°–41°N).

model. The tendency equation for CO in the model can be written approximately as

$$\frac{\partial \chi}{\partial t} = \text{advection} + \text{convection} + \text{chemistry}. \quad (1)$$

Here χ represents the CO mixing ratio, and the three terms on the right hand side represent three-dimensional advection from the large-scale meteorological fields, vertical transport due to parameterized convection, and net chemical production and loss. There are two additional terms in MOZART-4 associated with explicit diffusion and surface pressure tendency, but these are small and not discussed further. Convection is parameterized using the *Hack* [1994] scheme and the modified version of the *Zhang and McFarlane* [1995] scheme. More details regarding the effects of parameterized convection on tracers can be found in the work of *Hess* [2005]. The net chemical production of CO is controlled by the oxidation of methane and other volatile organic compounds (VOCs) to produce CO, balanced by its destruction by OH. We evaluated each of the individual terms in equation (1) using daily output from MOZART-4, and confirmed accurate balance (not shown); below we examine the specific balances of advection, parameterized convection and chemistry terms in the simulation.

[23] For the budget analysis, we focus on three geographical regions over Southeast Asia (Figure 11) to examine the importance of large-scale circulation and convection. Monthly mean outgoing longwave radiation (OLR) is used as proxy of deep convection [*Liebman and Smith*, 1996]. The "convective region" (region 1, red rectangle) is chosen where deep convection (low OLR) is dominant during NH summer (shading in Figure 11) and CO has a maximum at 215 hPa (Figure 2). Deep convection shows a maximum over the Bay of Bengal and South China Sea for June 2005, and this region is dominated by a strong low-level horizontal convergent flow from southwest (Figure 9). The west side of the CO maximum at 100 hPa, apart from the region of deep convection, is named the "anticyclone region" and is denoted by the blue rectangle (region 2). The region of the Tibetan Plateau is marked as a green rectangle (region 3), for the reasons discussed above.

[24] The time-averaged balance of terms in the tracer continuity equation (1) (i.e., advection, convection, and chemistry) is shown for the convective region in Figure 12c. Here the CO budget is a balance between strong positive tendencies from parameterized convection (between 500 and 200 hPa), and approximately equal parts negative advection and chemical loss. The negative advective tendency results from divergence of CO out of the convective region by the large-scale circulation, and much of this CO is transported in the middle and upper troposphere toward the east over the North Pacific Ocean (as seen in Figure 2). This northeastward transport of CO from the source regions is dominant in the midtroposphere up to about 200 hPa level (figures not shown). Figure 12d shows a time series of the budget balance at 200 hPa within the convective region, showing significant variability with maxima in convective transport balanced by (negative) maxima in advection; the net chemical production is a relatively constant weak loss.

[25] Figure 12a shows the time-averaged balance within the anticyclone region; note that the overall tendencies are much smaller than those within the convective region. In the troposphere there are small positive tendencies associated with advection and convection, balanced by chemistry. The (parameterized) convective forcing is near zero above 200 hPa, and the time average balance near 100 hPa shows advection balanced by chemical destruction. This relative magnitude of advection and convection is shown in the time series of the budget over this region at 100 hPa (Figure 12b). The advection results in transient increases and decreases with a positive time average, which is balanced by chemical destruction in long-term average. Note that the advection is associated with the resolved large-scale NCEP/GFS winds used in the MOZART-4, and in this case it is the large-scale upward motion on the eastern side of the anticyclone [*Park et al.*, 2007] that contributes to the net transport to 100 hPa. The overall balances within MOZART-4 thus show that (parameterized) convection is a primary mechanism of transport from the surface to the upper troposphere, but only to approximately 200 hPa. Transport to higher levels involves advection by the large-scale winds; in particular, the CO maximum at 100 hPa associated with the monsoon anticyclone is due to the resolved upward circulation in this region. The budget analysis over the Tibetan Plateau (not shown) reveals a shallow (weak) convective maximum near 400 hPa and negative advection in the middle troposphere. Together with the lack of surface sources of CO, the Tibetan Plateau does not have significant contribution to the maximum in the Asian monsoon anticyclone.

5. Summary and Discussion

[26] Observations of chemical constituents of tropospheric origin show persistent maxima inside the Asian monsoon anticyclone in the UTLS during NH summer [*Park et al.*, 2004, 2007; *Li et al.*, 2005]. This behavior is due to the vertical transport of lower tropospheric air by deep convection, and subsequent confinement within the monsoon anticyclone; these patterns are observed to extend into the lower stratosphere [*Park et al.*, 2008]. However, several aspects of the transport have been a topic of debate,

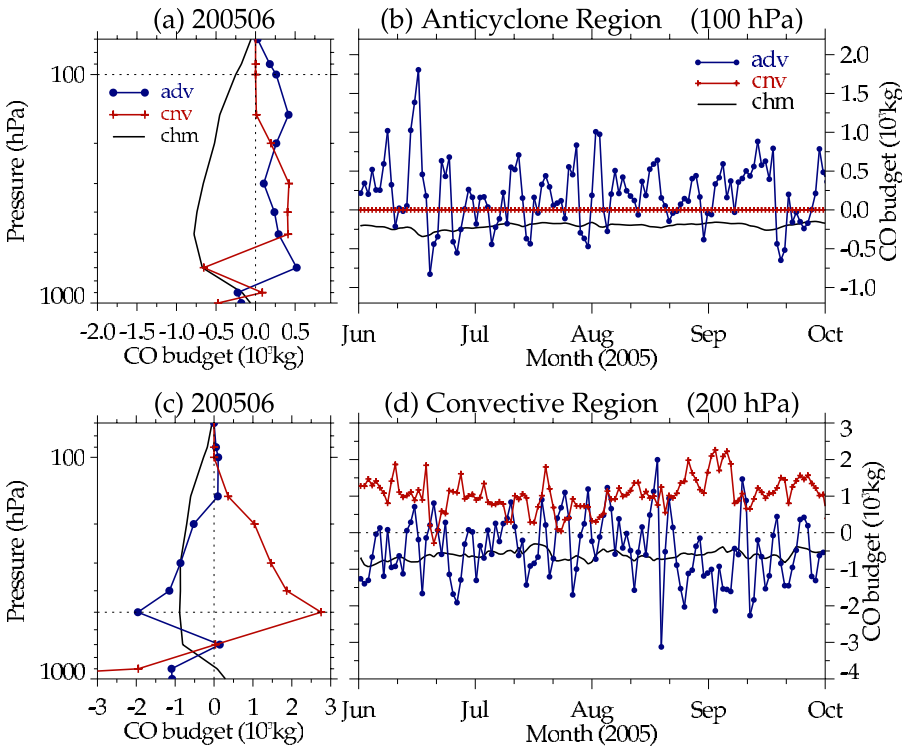

Figure 12. Average vertical profiles of CO budgets (advection, solid circles; convection, plusses; chemistry, solid line) in the model over (a) the anticyclone region (region 2) and (c) the convective region (region 1) in June 2005. Time series of CO advection (solid circles), convection (plusses), and chemistry (solid line) over (b) the anticyclone region at 100 hPa and (d) the convective region at 200 hPa from June to September 2005.

including the surface source regions [*Fu et al.*, 2006] and the mechanisms for transport above the level of main convective outflow [*Dessler and Sherwood*, 2004; *Park et al.*, 2007]. Here we have used simulations of CO from a global chemistry transport model (MOZART-4), incorporating tagged surface emission sources of CO and analyzed meteorological fields, to quantify transport and sources of CO in the Asian monsoon region during NH summer of 2005. The results of the simulation show overall good agreement with the space-time behavior of CO in the UTLS region observed by the MLS and ACE-FTS satellite instruments. In particular, the horizontal structure and temporal variability of the modeled CO are in reasonable agreement with the MLS data for the summer of 2005, and the vertical structure of the modeled CO over the region of the anticyclone exhibits a relative maximum near 15 km, in agreement with the average structure derived from ACE-FTS measurements. This overall agreement with observations prompts further analysis of the detailed transport pathways in the model.

[27] The surface source regions for CO inside the anticyclone at 100 hPa are identified using tagged emission regions. The results of the tagged run show that the contribution from the pollution sources over India and Southeast Asia, located close to the region of deep convection, directly contribute up to 30% of the CO at 100 hPa (Figure 10b). There are somewhat smaller contributions from the major polluted region of Eastern China (Figure 10a). Note that surface sources of CO contribute approximately half of the burden in the troposphere, with the other half arising from photochemical production. The contribution of surface CO emissions from the rest of the region to the anticyclone is small, and in particular there is almost no contribution from the Tibetan Plateau. The weak transport

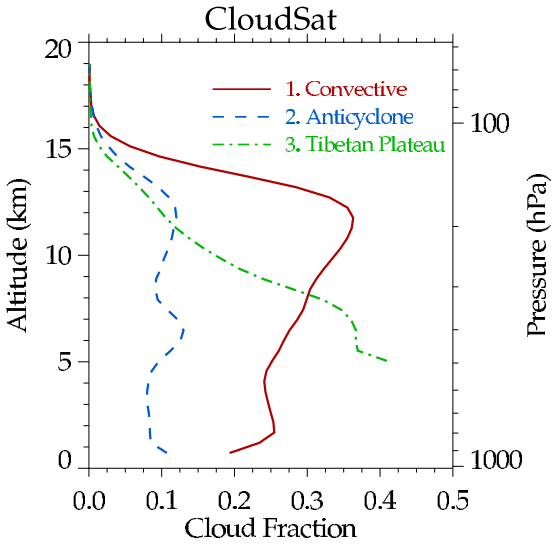

Figure 13. Vertical profiles of climatological cloud fraction over the Asian monsoon region, derived from CloudSat cloud profiling radar measurements. Observations from June to August 2006–2008 are used to calculate the fractional cloud occurrence for each of the geographical regions shown in Figure 11.

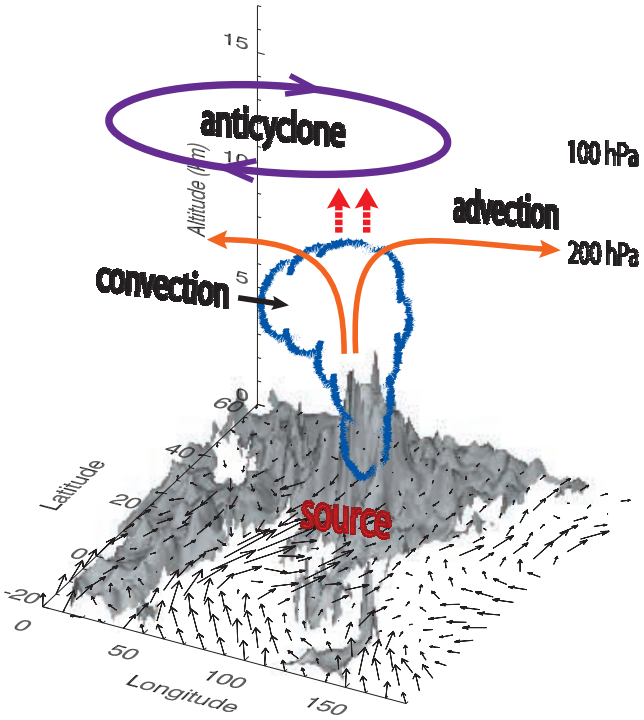

Figure 14. Schematic showing transport pathways over the Asian monsoon anticyclone. India and Southeast Asia are denoted as the most significant source region of the surface CO emission. A cloud over the southern slope of the Tibetan Plateau represents monsoon deep convection. Horizontal advection of CO at 200 hPa is shown as solid arrows (orange), and the large-scale vertical transport is shown as dashed arrows (red). The Asian monsoon anticyclonic circulation is shown as a solid line (purple) at 100 hPa. Surface wind vectors from the NCEP/NCAR reanalysis are overlaid on top of the topography.

from the region of the Tibetan plateau is due to the lack of surface emissions in this region (Figure 9), combined with an infrequent occurrence of deep convection reaching to the upper troposphere over Tibet. The lack of persistent deep convection over the Tibetan Plateau has been inferred from OLR statistics [*Park et al.*, 2007, Figure 2]. This behavior is confirmed (Figure 13) by CloudSat cloud profiling radar satellite measurements [*Stephens et al.*, 2008], which show very infrequent occurrence of convective clouds above 10 km over the Tibet region.

[28] Figure 14 shows a schematic diagram of transport in the Asian monsoon region diagnosed from the MOZART-4 results, including the location of convection (and strong surface convergence), the relevant surface emissions, and the Asian monsoon anticyclone over the topography of Asia. The model results show that enhanced UTLS CO in the monsoon region originates from strong convective transport, up to approximately the 200 hPa level. The majority of this air detrains in the upper troposphere, and is advected both toward the southwest (in the cross-equatorial Hadley circulation) and northeastward over the North Pacific Ocean (as discussed by *Jiang et al.* [2007]). Some fraction of the air is also advected vertically by the large-scale upward motion on the eastern side of the anticyclone [*Park et al.*, 2007], and much of the air that reaches the 100 hPa level is transported to the west and effectively confined within the anticyclonic circulation (to the northwest of the region of deep convection). Note that the closed anticyclonic circulation near 100 Pa is especially effective for confining air parcels, as quantified by *Randel and Park* [2006]. This transport behavior gives rise to the isolated CO maximum within the anticyclone, with a relative maximum in altitude near 15 km (e.g., Figure 8), and explains the relatively different horizontal structures observed for CO between 100 and 215 hPa (Figures 1–2).

[29] **Acknowledgments.** This work was partially supported by the National Aeronautics and Space Administration under the ACMAP and EOS programs. We thank Helen Worden and Jean-Francois Lamarque for discussions and comments on the manuscript. Andrew Gettelman and Jennifer Kay provided expertise on convective cloud behavior and easy access to the CloudSat satellite data. The Atmospheric Chemistry Experiment (ACE), also known as SCISAT, is a Canadian-led mission mainly supported by the Canadian Space Agency and the Natural Sciences and Engineering Research Council of Canada. We thank Peter Bernath, Kaley Walker, and Chris Boone for providing data set and helpful comments. Work at the Jet Propulsion Laboratory, California Institute of Technology, was under contract with NASA. The National Center for Atmospheric Research is operated by the University Corporation for Atmospheric Research under sponsorship of the National Science Foundation.

References

Bernath, P. F., et al. (2005), Atmospheric Chemistry Experiment (ACE): Mission overview, *Geophys. Res. Lett.*, *32*, L15S01, doi:10.1029/2005GL022386.

Bowman, K. P. (2006), Transport of carbon monoxide from the tropics to the extratropics, *J. Geophys. Res.*, *111*, D02107, doi:10.1029/2005JD006137.

Clerbaux, C., et al. (2007), CO measurements from the ACE-FTS satellite instrument: Data analysis and validation using ground-based, airborne and spaceborne observations, *Atmos. Chem. Phys.*, *8*, 2569–2594.

Connors, V., B. Gormsen, S. Nolf, and H. Reichle Jr. (1999), Spaceborne observations of the global distribution of carbon monoxide in the middle troposphere during April and October 1994, *J. Geophys. Res.*, *104*, 21,455–21,470, doi:10.1029/1998JD100085.

Dessler, A. E., and S. C. Sherwood (2004), Effect of convection on the summertime extratropical lower stratosphere, *J. Geophys. Res.*, *109*, D23301, doi:10.1029/2004JD005209.

Duncan, B. N., J. A. Logan, I. Bey, I. A. Megretskaia, R. M. Yantosca, P. C. Novelli, N. B. Jones, and C. P. Rinsland (2007), Global budget of CO, 1988–1997: Source estimates and validation with a global model, *J. Geophys. Res.*, *112*, D22301, doi:10.1029/2007JD008459.

Edwards, D. P., et al. (2003), Tropospheric ozone over the tropical Atlantic: A satellite perspective, *J. Geophys. Res.*, *108*(D8), 4237, doi:10.1029/2002JD002927.

Edwards, D. P., et al. (2006), Satellite-observed pollution from Southern Hemisphere biomass burning, *J. Geophys. Res.*, *111*, D14312, doi:10.1029/2005JD006655.

Folkins, I., S. J. Oltmans, and A. M. Thompson (2000), Tropical convective outflow and near surface equivalent potential temperature, *Geophys. Res. Lett.*, *27*(16), 2549–2552, doi:10.1029/2000GL011524.

Folkins, I., S. Fueglistaler, G. Lesins, and T. Mitovski (2008), A low-level circulation in the tropics, *J. Atmos. Sci.*, *65*, 1019–1034, doi:10.1175/2007JAS2463.1.

Fu, R., Y. Hu, J. S. Wright, J. H. Jiang, R. E. Dickinson, M. Chen, M. Filipiak, W. G. Read, J. W. Waters, and D. L. Wu (2006), Short circuit of water vapor and polluted air to the global stratosphere by convective transport over the Tibetan Plateau, *Proc. Natl. Acad. Sci. U. S. A.*, *103*, 5664–5669, doi:10.1073/pnas.0601584103.

Gettelman, A., M. L. Salby, and F. Sassi (2002), Distribution and influence of convection in the tropical tropopause region, *J. Geophys. Res.*, *107*(D10), 4080, doi:10.1029/2001JD001048.

Hack, J. J. (1994), Parameterization of moist convection in the NCAR Community Climate Model, CCM2, *J. Geophys. Res.*, *99*, 5551–5568, doi:10.1029/93JD03478.

Hess, P. G. (2005), A comparison of two paradigms: The relative global roles of moist convective versus nonconvective transport, *J. Geophys. Res.*, *110*, D20302, doi:10.1029/2004JD005456.

Highwood, E. J., and B. J. Hoskins (1998), The tropical tropopause, *Q. J. R. Meteorol. Soc.*, *124*, 1579–1604, doi:10.1002/qj.49712454911.

Horowitz, L. W., et al. (2003), A global simulation of tropospheric ozone and related tracers: Description and evaluation of MOZART, version 2, *J. Geophys. Res.*, *108*(D24), 4784, doi:10.1029/2002JD002853.

Hoskins, B. J., and M. J. Rodwell (1995), A model of the Asian summer monsoon. part I: The global scale, *J. Atmos. Sci.*, *52*, 1329–1340, doi:10.1175/1520-0469(1995)052<1329:AMOTAS>2.0.CO;2.

Jiang, J. H., N. J. Livesey, H. Su, L. Neary, J. C. McConnell, and N. A. D. Richards (2007), Connecting surface emissions, convective uplifting, and long-range transport of carbon monoxide in the upper troposphere: New observations from the Aura Microwave Limb Sounder, *Geophys. Res. Lett.*, *34*, L18812, doi:10.1029/2007GL030638.

Kinnison, D. E., et al. (2007), Sensitivity of chemical tracers to meteorological parameters in the MOZART-3 chemical transport model, *J. Geophys. Res.*, *112*, D20302, doi:10.1029/2006JD007879.

Kistler, R., et al. (2001), The NCEP/NCAR 50-year reanalysis: Monthly means CDROM and documentation, *Bull. Am. Meteorol. Soc.*, *82*, 247–267, doi:10.1175/1520-0477(2001)082<0247:TNNYRM>2.3.CO;2.

Lelieveld, J., et al. (2002), Global air pollution crossroads over the Mediterranean, *Science*, *298*, 794–799, doi:10.1126/science.1075457.

Li, Q., et al. (2005), Trapping of Asian pollution by the Tibetan anticyclone: A global CTM simulation compared with EOS MLS observations, *Geophys. Res. Lett.*, *32*, L14826, doi:10.1029/2005GL022762.

Liebman, B., and C. A. Smith (1996), Description of a complete (interpolated) outgoing longwave radiation dataset, *Bull. Am. Meteorol. Soc.*, *77*, 1275–1277.

Liu, C., and E. J. Zipser (2005), Global distribution of convection penetrating the tropical tropopause, *J. Geophys. Res.*, *110*, D23104, doi:10.1029/2005JD006063.

Livesey, N. J., et al. (2007), Version 2.2 level 2 data quality and description document, report, NASA Goddard Earth Sci. Distrib. Active Arch. Cent., Pasadena, Calif.

Livesey, N. J., et al. (2008), Validation of Aura Microwave Limb Sounder O_3 and CO observations in the upper troposphere and lower stratosphere, *J. Geophys. Res.*, *113*, D15S02, doi:10.1029/2007JD008805.

Logan, J. A., M. J. Prather, S. C. Wofsy, and M. B. McElroy (1981), Tropospheric chemistry—A global perspective, *J. Geophys. Res.*, *86*, 7210–7254, doi:10.1029/JC086iC08p07210.

Marenco, A., H. Gouget, P. Nedelec, J. P. Pages, and F. Karcher (1994), Evidence for long term tropospheric ozone increase from Pic Du Midi series—consequences: Positive radiative forcing, *J. Geophys. Res.*, *99*, 16,617–16,632, doi:10.1029/94JD00021.

Nedelec, P., V. Thouret, J. Brioude, B. Sauvage, J.-P. Cammas, and A. Stohl (2005), Extreme CO concentrations in the upper troposphere over northeast Asia in June 2003 from the in situ MOZAIC aircraft data, *Geophys. Res. Lett.*, *32*, L14807, doi:10.1029/2005GL023141.

Novelli, P. C., K. A. Masarie, and P. M. Lang (1998), Distributions and recent changes of carbon monoxide in the lower troposphere, *J. Geophys. Res.*, *103*(D15), 19,015–19,033, doi:10.1029/98JD01366.

Novelli, P. C., K. A. Masarie, P. M. Lang, B. D. Hall, R. C. Myers, and J. W. Elkins (2003), Re-analysis of tropospheric CO trends: Effects of the 1997–1998 wildfires, *J. Geophys. Res.*, *108*(D15), 4464, doi:10.1029/2002JD003031.

Park, M., W. J. Randel, D. E. Kinnison, R. R. Garcia, and W. Choi (2004), Seasonal variation of methane, water vapor, and nitrogen oxides near the tropopause: Satellite observations and model simulations, *J. Geophys. Res.*, *109*, D03302, doi:10.1029/2003JD003706.

Park, M., W. J. Randel, A. Gettelman, S. T. Massie, and J. H. Jiang (2007), Transport above the Asian summer monsoon anticyclone inferred from Aura Microwave Limb Sounder tracers, *J. Geophys. Res.*, *112*, D16309, doi:10.1029/2006JD008294.

Park, M., W. J. Randel, L. K. Emmons, P. F. Bernath, K. A. Walker, and C. D. Boone (2008), Chemical isolation in the Asian monsoon anticyclone observed in Atmospheric Chemistry Experiment (ACE-FTS) data, *Atmos. Chem. Phys.*, *8*, 757–764.

Randel, W. J., and M. Park (2006), Deep convective influence on the Asian summer monsoon anticyclone and associated tracer variability observed with Atmospheric Infrared Sounder (AIRS), *J. Geophys. Res.*, *111*, D12314, doi:10.1029/2005JD006490.

Schoeberl, M. R., et al. (2006), Overview of the EOS aura mission, *IEEE Trans. Geosci. Remote Sens.*, *44*, 1066–1074, doi:10.1109/TGRS.2005.861950.

Stephens, G. L., et al. (2008), CloudSat mission: Performance and early science after the first year of operation, *J. Geophys. Res.*, *113*, D00A18, doi:10.1029/2008JD009982.

van der Werf, G. R., J. T. Randerson, L. Giglio, G. J. Collatz, P. S. Kasibhatla, and A. F. Arellano Jr. (2006), Interannual variability in global biomass burning emissions from 1997 to 2004, *Atmos. Chem. Phys.*, *6*, 3423–3441.

Velazco, V., et al. (2007), Annual variation of strato-mesospheric carbon monoxide measured by ground-based Fourier transform infrared spectrometry, *Atmos. Chem. Phys.*, *7*, 1305–1312.

Waters, J. W., et al. (2006), The Earth Observing System Microwave Limb Sounder (EOS MLS) on the Aura satellite, *IEEE Trans. Geosci. Remote Sens.*, *44*, 1075–1092, doi:10.1109/TGRS.2006.873771.

Xiao, Y., D. J. Jacob, and S. Turquety (2007), Atmospheric acetylene and its relationship with CO as an indicator of air mass age, *J. Geophys. Res.*, *112*, D12305, doi:10.1029/2006JD008268.

Zhang, G. J., and N. A. McFarlane (1995), Sensitivity of climate simulations to the parameterization of cumulus convection in the Canadian Climate Centre general circulation model, *Atmos. Ocean*, *33*, 407–446.

L. K. Emmons, M. Park, and W. J. Randel, Atmospheric Chemistry Division, National Center for Atmospheric Research, P.O. Box 3000, Boulder, CO 80307-3000, USA. (mijeong@ucar.edu)

N. J. Livesey, Jet Propulsion Laboratory, California Institute of Technology, Pasadena, CA 91109, USA.